

1. Radiative transfer

The radiative transfer code²⁶ reproduces the Jovian reflectivity including the gaseous absorption by methane²⁷⁻²⁸, Rayleigh scattering by H₂ and He, and absorption and scattering by particles modelled with Mie phase functions²⁹. We fitted simultaneously the observations to a model of the centre to limb reflectivity in 7 wavelengths ranging from ultraviolet (275nm) to near infrared (953 nm), including methane absorption bands at 890 nm and 2.3 μ m. Table S1 summarizes the free and fixed parameters used to reproduce the observed pre-, during and after-disturbance reflectivity. Free parameters were scanned within the showed ranges at the corresponding modelling step (second column), while parameters in the fourth column were assumed to have constant values. We show in Figure S1 an example of best-fitting results for June 5 HST observations.

Table S1: Vertical cloud structure model parameters

| Layer | Free Parameters | Step | Fixed Parameters |
|--------------------|--|-------------------------------|--|
| Stratospheric haze | $P_{\text{bot}}=10\text{--}100$ mbar $\tau=0\text{--}1.5$ $m_i=-0.5\text{--}-0.0005$ $a=0.04\text{--}0.1$ μ m | 10mbar 0.01 10X 0.01 | $P_{\text{top}}=1$ mbar $m_r=1.43$ $b=0.1$ |
| Tropospheric haze | $P_{\text{top}}=100\text{--}500$ mbar $\tau=0\text{--}10$ $m_i=-0.5\text{--}-0.0005$ $a=0.1\text{--}1.0$ μ m | 10mbar 1 10X 0.1 | $P_{\text{bot}}=700$ mbar $m_r=1.43$ $b=0.1$ |
| Bottom cloud | $\varpi_0=0.90\text{--}1.0$ | 0.01 | $P=700$ mbar |

Notes: P_{top} =top pressure; P_{bot} =bottom pressure; τ =optical thickness of the layer; m_r =real refractive index; m_i =imaginary refractive index; a =mean size of the Hansen's distribution; b =width of the Hansen's size distribution; ϖ_0 =single scattering albedo of the isotropic particles; 10X=ten-fold variation of the parameter .

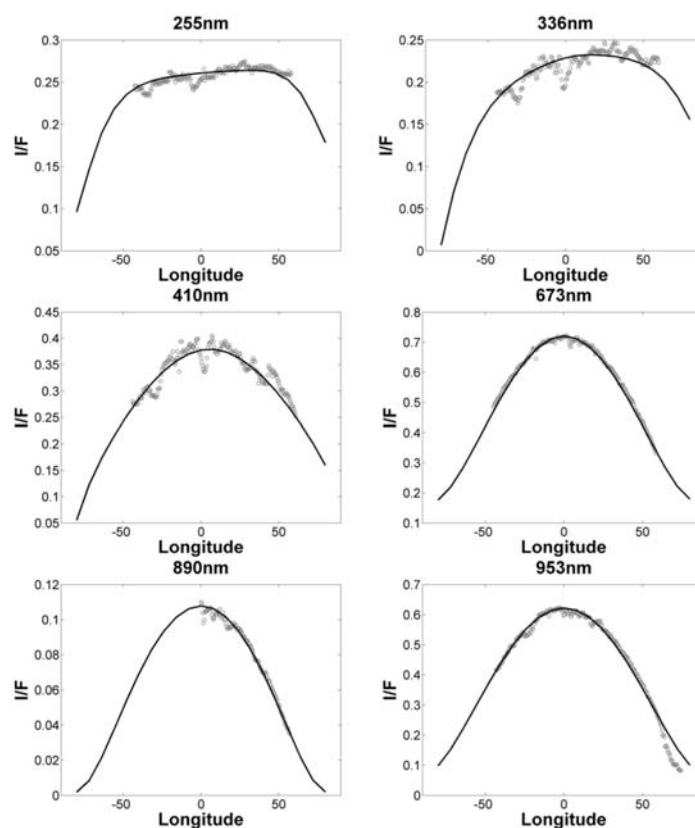


Figure S1: Best-fitting models for June 5 HST observations. Grey points show the absolute I/F (reflectivity) measured in HST images and the black line is used for results of a given vertical cloud structure model in all available wavelengths.

Figure S2 shows the downward solar radiation flux calculated with a doubling-adding technique³⁰ in the 0.25 – 1.0 μm range. The computation assumes a realistic Jupiter vertical cloud and haze structure as determined above. This spectral range accounts for about 70% of the incident solar flux at the top of the atmosphere. About half of the remaining infrared radiation is absorbed by methane also at high altitudes. This shows that most of the solar energy is deposited above the 1 bar level. Only about 15% of the total incident daily flux could reach the NH_4SH cloud at 2 bar. This constrains the solar radiation deposition level to the upper troposphere.

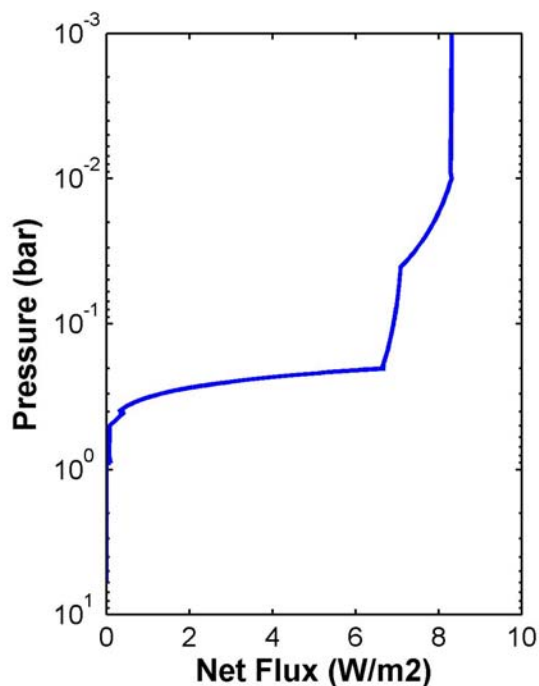


Figure S2: Downward daily solar radiation flux in the 0.25 – 1.0 μm range.

2. Wind measurements

Wind measurements on HST images (mostly at a wavelength of 410 nm) were done by visually identifying and tracking cloud features in pair of images separated by a planetary rotation (10 hr) and by using an automatic one-dimensional correlator¹¹. The typical rms error for the measured jet velocity was 5 ms^{-1} . The IOPW images were used to visually measure the disturbance motions with a temporal span from 3 to 45 days. Typical velocity errors of the plumes were in the range of $0.5\text{--}2 \text{ ms}^{-1}$ (figure S3) while disturbance features had errors of 15 ms^{-1} due to lower tracking time intervals.

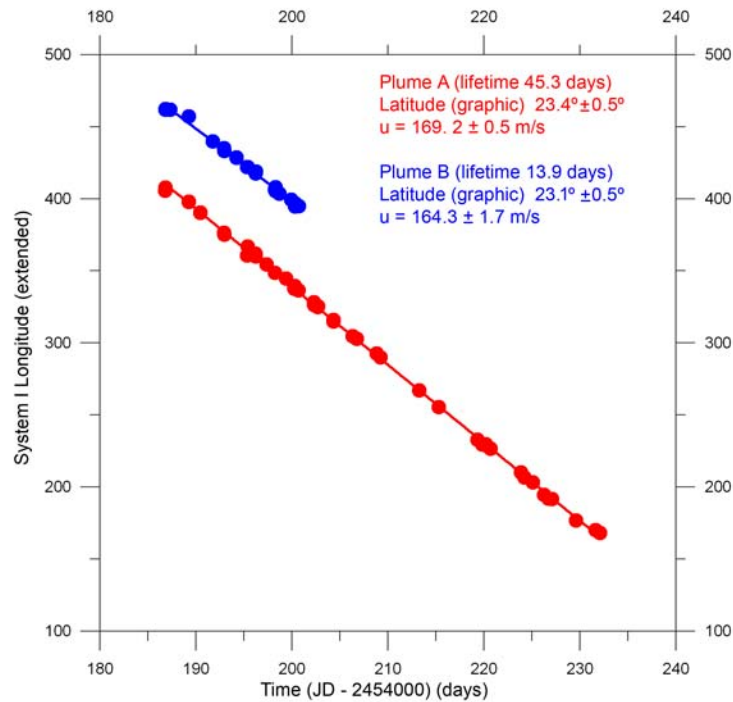


Figure S3. Plumes track and drift rate in the reference longitude System I (rotation period = 9 hr 50 min 30.003 sec). Red = plume A; Blue: plume B. The latitude (planetographic) and the zonal wind speed (u) relative to System III (rotation period 9 hr 55 min 29.711 s) is indicated for both plumes. JD is the Julian Date time.

The “image stacking” procedure used by the IOPW team consists in shift and adding the best images of a series obtained in a short temporal exposure employing CCD “webcams” and software such as “RegiStax”. This technique applies successfully to bright objects like the planets and improves the image quality in some cases to the diffraction limit³¹⁻³³. In our case the technique was validated from a comparison of simultaneous images obtained with the HST and by the IOPW team.

3. Convective model

The convective simulations were run in a domain extending vertically from 15 bar to 2 mbar with a spatial resolution of 2 km per grid point in a model domain of 170x170 km x 230 km vertically. Boundary conditions were free-slipping on the lateral sides and the bottom boundary while damping of gravity waves was introduced on the upper layers. A sub-grid scale parameterization of turbulence was also incorporated¹⁷. The simulations assumed different abundances of water and a 3 times solar abundance of NH₃ and SH₂. The modeled atmosphere has a relative humidity of 95 % for all condensates and a normal ortho-para hydrogen distribution. The thermal profile is extended downward from the 1 bar level following a dry adiabat that takes into account the varying atmospheric composition with humidity. Convection was triggered by a thermal perturbation of 0.5 K at the water condensation level with a gaussian shape and size of 6 km. We considered that all condensates fully precipitate. Typical storms grew to a fully convective updraft from the water cloud base to the uppermost levels in a time-scale of 2 hours. The average ascending velocity in the simulated convective cell was 130 m/s.

The interaction of the storm with the jet was simulated using a 2D model with a spatial resolution of 5 km over a 10,000 x 5,000 km area. The code considers a divergence source where material is injected as a passive tracer representing the plume and takes into account mass continuity, advection and Coriolis forces to simulate the turbulent material following the plume²². The 2D model is initialized with parameters from the 3D simulation (mass detrainment at the visible cloud level with outward motions on the order of 50 m/s at 100 km from the storm central axis).

4. EPIC model

The EPIC model²³ solves numerically the primitive equations of meteorology in spherical geometry. It gives, among other field variables, the potential vorticity distribution which is a dynamical variable that is conserved in an inviscid and adiabatic flow, and can be used as a flow tracer. The free parameters in this model are the vertical profiles of temperature and zonal wind. Above the tropospheric cloud (level P_0) we used the thermal profile obtained from radio occultation experiments¹⁹; below cloud tops, the thermal profile was extrapolated by a wet adiabat characterized by the value of the static stability of the lower levels. The three-dimensional structure of the wind field is separated as a product of two functions $a(p) u(y)$ where $u(y)$ is the wind profile at the cloud tops and $a(p)$ is a nondimensional amplitude factor. For $a(p)$, we adopted a two-segment linear approach²⁴. Above the P_0 level, the winds decrease according to the thermal wind equation²¹ and below P_0 (increasing pressure), the profile was extrapolated down to a turning point P_1 where the wind shear is defined as $a(p) = 1 + m \ln (p/p_1)$ and becomes positive, negative or zero, depending on values of the free parameter m , representing increasing, decreasing or constant winds²⁴. Table S2 summarizes the characteristics of the simulations. Results were very sensitive to the shape of the initial wind profile shape. Turbulence was easily created on the 25 march profile by adding a heat pulse on the model but not on the June 5 profile which was stable to the same heat pulses. Only positive values of m (winds increasing in depth) resulted in stable simulations for the March profiles.

Table S2: Summary of EPIC model simulations.

| Model domain and resolution | |
|---|--|
| Latitude range | +16° to +31° |
| Longitude range | 120° |
| Resolution | 0.23°/pixel |
| Number of vertical layers | 7, 8, 10 |
| Simulated winds structure | |
| Simulated profiles: $u(y)$ | March 25 2007; June 5 2007 |
| Reference pressure: P_0 | 600 mbar |
| Wind inflexion level: P_I | 600, 1000, 2500 mbar |
| Vertical shear: m (e-folding) | -0.42, -0.25, -0.1, 0.0, 0.1, 0.25, 0.42 |
| Thermal structure | |
| Temperature profile | $N = 0.0010 \text{ s}^{-1}$ |
| Notes: The 0.42 value of m corresponds to a prolongation of the vertical shear observed by the Voyagers. | |

Supplementary Notes

26. Sánchez-Lavega A., Hueso R. and Pérez-Hoyos S. The three-dimensional structure of Saturn's equatorial jet at cloud level. *Icarus* **187**, 510 – 519 (2007).
27. Karkoschka, E. Methane, ammonia and temperature measurements of the jovian planets and Titan from CCD-spectrophotometry. *Icarus* **133**, 134 – 146 (1998).
28. Irwin P.G.J., Sromovsky L.A., Strong E.K., Sihra K., Teanby N.A., Bowles N., Calcutt S.B., and Remedios J.J. Improved near-infrared methane band models and k-distribution parameters from 2000 to 9500 cm⁻¹ and implications for interpretation of outer planet spectra. *Icarus* **181**, 309 – 319 (2006).
29. West, R.A., Baines K.H., Friedson A.J., Banfield D., Ragent B., and F.W. Taylor. Jovian clouds and haze in Jupiter: The planet, satellites and magnetosphere, Eds. F. Bagenal, T.E. Dowling and W.B. McKinnon Cambridge University Press (UK) pp. 79 – 104 (2004).
30. Pérez-Hoyos, S. and A. Sánchez-Lavega, Solar flux in Saturn's atmosphere: penetration and heating rates in the aerosol and cloud layers. *Icarus* **180**, 368 – 378 (2006).
31. Dantowich, R. F., W. T. Scott and M. J. Kozubal. Ground-based high-resolution imaging of Mercury. *Astron. J.*, **119**, 2455-2457 (2000).
32. Baumgardner J., M. Mendillo, and J. K. Wilson. A digital high-definition imaging system for spectral studies of extended planetary atmospheres. I. Initial results in white light showing features on the hemisphere of Mercury unimaged by Mariner 10. *Astron. J.*, **119**, 2458-2464 (2000)
33. Wöhler C., R. Lena, P. Lazzarotti, J. Phillip, M. Wirths, Z. Pujic, and Geologic Lunar Research (GLR) Group. A combined spectrophotometric and morphometric study of the lunar mare dome fields near Cauchy, Arago, Hortensius, and Milichius. *Icarus*, **186**, 237-264 (2006).